 CMES, vol.24, no.3, pp.185-202, 2008

Coupled Atomistic/Continuum Simulation based on Extended Space-Time Finite Element Method

Shardool U. Chirputkar[1] **and Dong Qian**[2]

Abstract: A multiscale method based on the extended space-time finite element method is developed for the coupled atomistic/continuum simulation of nanoscale material systems. Existing single scale approach such as the finite element method has limited capability of representing the fine scale physics in both the spatial and temporal domains. This is a major disadvantage for directly incorporating FEM in coupled atomistic/continuum simulations as it results in errors such as spurious wave reflections at the atomistic/continuum interface. While numerous efforts have been devoted to eliminating the interfacial mismatch effects, less attention has been paid to developing fine scale, atomistic level representations within the FEM framework. In this paper, we show that multiscale space-time approximations can be established within the context of FEM. By augmenting the regular space-time finite element shape function basis with the enrichment function, we demonstrate that the continuum and atomistic representations can be consistently linked and this naturally leads to a reflectionless interfacial boundary condition. In addition, a unique feature of this approach is its ability to achieve wave transmitting condition that is energy conservative. Realization of these properties is illustrated through both harmonic and nonlinear lattices in 1D.

Keyword: Multiscale simulation, enrichment, X-FEM, X-TFEM, VAC model, reflectionless interface

[1] Department of Mechanical Engineering, University of Cincinnati, Cincinnati, OH 45221.

[2] Corresponding Author. Department of Mechanical Engineering, University of Cincinnati, Cincinnati, OH 45221. Email dong.qian@uc.edu

1 Introduction

Even with its tremendous success in modeling material systems and devices, simulation based on full-scale atomistic description is still an expensive technique and thus limited in the relevant spatial and temporal scales it can address. In this context, multiscale method based on coupled atomistic/continuum simulation offers the unique advantage of arriving at the solution with enormous computational saving. It also provides a robust computing platform for applications that are of multiscale in nature. Examples include materials with hierarchical structures and components, crack propagation, dislocation-induced plasticity, and many others. In implementing coupled atomistic/continuum simulations, one critical issue is the development of robust representations of energy and momentum in the respective continuum and atomistic regions. Another important challenge is the accurate account on information exchange between the domains across the interface. A lack of consistent link between the continuum and atomistic models leads to spurious phonon reflections at the atomistic/continuum interface, which subsequently pollutes the numerical solution.

A large amount of work has recently been devoted to the interface in coupled atomistic/continuum simulations. Significant developments include the Langevin approach by Cai, de Koning, Bulatov, and Yip (2000) for linear systems. The Bridging-scale method (BSM) has been proposed by Wagner and Liu (2003) and extended in (Park, Karpov, Liu, and Klein (2005); Qian, Wagner, and Liu (2004); Wagner, Karpov, and Liu (2004); Karpov, Yu, Park, Liu, Wang, and Qian (2006)) based on projection operator and Langevin type of time-history kernel. E and Huang (2001, 2002) de-

rived a procedure for coupling molecular dynamics with linear elasticity based on the minimization of reflections. Xiao and Belytschko (2004) have developed a bridging domain formulation in which the compatibility between finite element and molecular dynamics degree of freedoms are enforced based on constraints using Lagrangian multipliers. The energy conserving properties of the bridging domain formulation are presented by Belytschko (2007) and more recently in (Xu and Belytschko (2008)). To and Li (2005); Li, Liu, Agrawal, and To (2005) proposed the perfectly matched layer (PML) method by matching the impedance at the atomistic/continuum interface. Application of PML for non-equilibrium molecular dynamics was demonstrated by Liu and Li (2007).

Since the continuum description is typically based on finite element with mesh size much larger than the atomic spacing, the FEM approximation is not capable of describing the phonons with length scales smaller than the size of the mesh. As such, the fine scale phonons that are originated from the atomistic region get reflected at the numerical interface of the FEM and atomistic simulation. To remove such spurious reflections, one solution is to impose damping mechanism at the interface so that the fine scale phonons originated from the atomistic simulation are effectively dissipated. The corresponding boundary condition is sometimes referred to as the reflectionless boundary condition. This approach is effective if the atomistic description is limited to a single domain. Considering, however, the case of atomistic descriptions used in multiple domains, the damping-based methodology may have difficulties as the fine scale phonons originated from each domain need to propagate through the continuum region to interact with each other. Although the imposed damping eliminates the reflection, it also dissipates the fine scale components of the wave that need to be transmitted through the continuum region. The lack of representation of the fine scale behavior in the continuum region could further lead to erroneous simulation results.

In this paper, we present a multiscale method based on coupling the extended space-time finite element method with atomistic simulation. We show that the reflectionless boundary condition can be achieved by establishing accurate representations of the scale phonons in the continuum region based on an enrichment method. In addition, it naturally leads to a wave transmitting condition that is energy conservative. The proposed approach has three key components: the space-time finite element method for discrete atomic systems, the multiscale approximation based on enrichment and coupling with atomistic simulation methods. Integrating these three components allows us to address the fine scale phenomena in both the spatial and temporal domains. To the best of our knowledge, the method proposed is the first of its kind for treating the interfaces in coupled atomistic/continuum simulation. The details of the implementation are outlined in the rest of the paper, which are organized as follows: The space-time finite element formulation for discrete atomic system is derived in section 2. The multiscale enrichment approximation for the space-time FEM formulation is presented in section 3. In section 4, we discuss the coupling of the extended space-time FEM method with atomistic simulation method. Example problems are provided in section 5 and a comparison with the existing approach is made. Final conclusions are presented in section 6.

2 The Space-time Finite Element Method

2.1 Basic Formulation

The idea of developing approximations in time using FEM shape functions is first proposed in (Argyris and Scharpf (1969); Fried (1969); Oden (1969); Gurtin (1964)), and among others. Detailed studies for wave propagation in continuum systems using space-time method can be found in (Hughes and Stewart (1996); Li and Wiberg (1996); Hulbert and Hughes (1990)). Recently, Chessa and Belytschko (2004) have developed a space-time version of the extended finite element method for capturing arbitrary discontinuities in continuum systems. Similar to (Chessa and Belytschko (2004)), the formulation to be described below is also based on the enrichment approach.

We have, however, limited our attention to the application to discrete atomic systems and coupling with atomistic simulations. A discontinuous Galerkin approach (Hughes and Stewart (1996); Zienkiewicz, Taylor, Sherwin, and Peiro (2003)) has been employed in this work, i.e., the space-time domain is decomposed into sub-domains and then variational principles are established within each sub-domain. While we have focused on continuous approximations, the formulation also allows for discontinuous representations in space and time.

Compared with the semi-discrete schemes, an important difference in the space-time formulation is that the approximations are built simultaneously in space and time. If finite element method is used, we have the following approximation in the space-time description for a general three-dimensional case

$$\mathbf{u}(\mathbf{x},t) = \sum_I \mathbf{N}_I(\mathbf{x},t)\mathbf{d}_I \tag{1}$$

in which $\mathbf{N}_I(\mathbf{x},t)$ is the finite element shape function defined at the space-time node indexed by I and evaluated at spatial coordinate $\mathbf{x}$ and time t. $\mathbf{d}_I$ is the corresponding space-time nodal degree of freedom. Note that although $\mathbf{N}_I$ and $\mathbf{d}_I$ look similar to the ones in the semi-discrete scheme, they are defined on a space-time grid as opposed to space only. For the purpose of simplicity, we will use the 2D space-time grid plotted in Figure 1 as a reference. The derived formulation, however, is not restricted to 2D. We consider a space-time domain Q, which is the Cartesian product of space domain Ω and time duration $(0,T)$, i.e., $Q = \Omega \times (0,T)$. The time domain is subdivided into time slabs with the n-th time slab given as $Q_n = \Omega \times (t_n, t_{n+1})$. The space time grid is discontinuous in time and $t^{\pm} = t \pm \varepsilon$ represents the discontinuity at time t, ε being an infinitesimal perturbation in time. The discontinuity in a variable $\mathbf{u}$ at time t is given by:

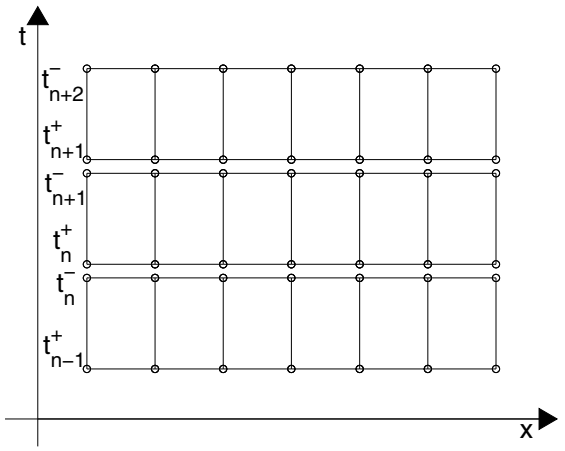

Figure 1: An illustration of a typical space-time grid used for a one-dimensional problem

$$[\![\mathbf{u}(t)]\!] = \mathbf{u}(t^+) - \mathbf{u}(t^-) \tag{2}$$

We consider an atomistic system in which the motion of the atoms obeys Newton's second law, i.e.,

$$\mathbf{G}\hat{\delta}(\mathbf{x} - \mathbf{x}_\alpha) = \mathbf{0} \tag{3}$$

where $\mathbf{G} = \mathbf{f}^{\mathbf{ext}} + \mathbf{f}^{\mathbf{int}} - m\ddot{\mathbf{u}}$ is a vector function of space coordinate $\mathbf{x}$ and $\hat{\delta}$ is the Dirac delta function. For the α-th atom, $\mathbf{f}^{\mathbf{ext}}_\alpha$ and $\mathbf{f}^{\mathbf{int}}_\alpha$ are the external and internal forces respectively. m_α, $\mathbf{x}_\alpha$ and $\ddot{\mathbf{u}}_\alpha$ correspond to the mass, position and acceleration of the α-th atom. The internal forcing term in Eq.(3) is governed by the inter-atomic potential W, i.e., $\mathbf{f}^{\mathbf{int}}_\alpha = -\partial W / \partial \mathbf{x}_\alpha$. Similar to the continuum case in (Hughes and Stewart (1996)), a space-time weak form employing discontinuous Galerkin formulation for the atomic system can be derived as:

$$\begin{aligned}
0 &= B(\delta\mathbf{u}^h, \mathbf{u}^h)_n - L(\delta\mathbf{u}^h)_n \\
&= \int_{Q_n} \delta\dot{\mathbf{u}}^{\mathbf{h}} \cdot \mathbf{G} \sum_{\alpha=1}^{N_a} \hat{\delta}(\mathbf{x} - \mathbf{x}_\alpha)\, dQ_n \\
&- \int_\Omega \delta\dot{\mathbf{u}}^{\mathbf{h}}(t_n^+) \cdot \left[\!\!\left[m\dot{\mathbf{u}}^{\mathbf{h}} \sum_{\alpha=1}^{N_a} \hat{\delta}(\mathbf{x} - \mathbf{x}_\alpha) \right]\!\!\right]_{t=t_n} d\Omega \\
&+ \int_\Omega \delta\mathbf{u}^{\mathbf{h}}(t_n^+) \cdot \left[\!\!\left[\mathbf{f}^{\mathbf{int}} \sum_{\alpha=1}^{N_a} \hat{\delta}(\mathbf{x} - \mathbf{x}_\alpha) \right]\!\!\right]_{t=t_n} d\Omega \\
&+ \int_\Omega \delta\mathbf{u}^{\mathbf{h}}(t_n^+) \cdot \left[\!\!\left[\mathbf{f}^{\mathbf{ext}} \sum_{\alpha=1}^{N_a} \hat{\delta}(\mathbf{x} - \mathbf{x}_\alpha) \right]\!\!\right]_{t=t_n} d\Omega
\end{aligned} \tag{4}$$

with

$$
\begin{aligned}
&B(\delta\mathbf{u}^{\mathbf{h}},\mathbf{u}^{\mathbf{h}})_n \\
&= -\int_{I_n}\int_{\Omega}\delta\dot{\mathbf{u}}^{\mathbf{h}}\left(m\ddot{\mathbf{u}}^{\mathbf{h}}\sum_{\alpha=1}^{N_a}\hat{\delta}(\mathbf{x}-\mathbf{x}_\alpha)\right)d\Omega\,dt \\
&\quad+\int_{I_n}\int_{\Omega}\delta\dot{\mathbf{u}}^{\mathbf{h}}\left(\mathbf{f}^{\mathbf{int}}\sum_{\alpha=1}^{N_a}\hat{\delta}(\mathbf{x}-\mathbf{x}_\alpha)\right)d\Omega\,dt \\
&\quad-\int_{\Omega}\delta\dot{\mathbf{u}}^{\mathbf{h}}(t_n^+)\left[m\dot{\mathbf{u}}^{\mathbf{h}}\sum_{\alpha=1}^{N_a}\hat{\delta}(\mathbf{x}-\mathbf{x}_\alpha)\right]_{t=t_n^+}d\Omega \\
&\quad+\int_{\Omega}\delta\mathbf{u}^{\mathbf{h}}(t_n^+)\left[\mathbf{f}^{\mathbf{int}}\sum_{\alpha=1}^{N_a}\hat{\delta}(\mathbf{x}-\mathbf{x}_\alpha)\right]_{t=t_n^+}d\Omega \qquad (5)
\end{aligned}
$$

$$
\begin{aligned}
&L(\delta\mathbf{u}^{\mathbf{h}})_n \\
&= -\int_{I_n}\int_{\Omega}\delta\dot{\mathbf{u}}^{\mathbf{h}}\left(\mathbf{f}^{\mathbf{ext}}\sum_{\alpha=1}^{N_a}\hat{\delta}(\mathbf{x}-\mathbf{x}_\alpha)\right)d\Omega\,dt \\
&\quad-\int_{\Omega}\delta\dot{\mathbf{u}}^{\mathbf{h}}(t_n^+)\left[m\dot{\mathbf{u}}\sum_{\alpha=1}^{N_a}\hat{\delta}(\mathbf{x}-\mathbf{x}_\alpha)\right]_{t=t_n^-}d\Omega \\
&\quad+\int_{\Omega}\delta\mathbf{u}^{\mathbf{h}}(t_n^+)\left[\mathbf{f}^{\mathbf{int}}\sum_{\alpha=1}^{N_a}\hat{\delta}(\mathbf{x}-\mathbf{x}_\alpha)\right]_{t=t_n^-}d\Omega \\
&\quad-\int_{\Omega}\delta\mathbf{u}^{\mathbf{h}}(t_n^+)\cdot\left[\!\!\left[\mathbf{f}^{\mathbf{ext}}\sum_{\alpha=1}^{N_a}\hat{\delta}(\mathbf{x}-\mathbf{x}_\alpha)\right]\!\!\right]_{t=t_n}d\Omega \qquad (6)
\end{aligned}
$$

in which $\delta\mathbf{u}^{\mathbf{h}}$ is the test function, δ is the variational sign and $I_n=(t_n,t_{n+1})$. N_a is the total number of atoms in the domain. Superscript h indicates the numerical approximation. The three terms on the right hand side of Eq.(4) represent the enforcement of momentum balance, velocity and displacement continuity condition, respectively. The direct substitution of the space-time FEM approximation into the bilinear weak form leads to a stiffness equation in the form of,

$$\mathbb{K}_n\overline{\mathbf{d}}_{n+1}=\mathbb{L}_n\overline{\mathbf{d}}_n+(\mathbb{L}_{ext})_n \qquad (7)$$

where

$$
\begin{aligned}
\mathbb{K}_n &= \mathbb{K}_{kin}+\mathbb{K}_{int}+\mathbb{K}_{kin}^+ +\mathbb{K}_{int}^+ && (8)\\
\mathbb{L}_n &= \mathbb{L}_{kin}^- +\mathbb{L}_{int}^- && (9)
\end{aligned}
$$

Here $\mathbb{K}_n$ is the space-time stiffness for the n-th time slab and is contributed by the kinetic and internal energy terms. The factor of $\mathbb{L}_n$ represents the information flux coming from the previous time slab and $(\mathbb{L}_{ext})_n$ represents the contribution from the external forces during the n^{th} time slab. We consider the case of a one-dimensional harmonic lattice and assume nearest neighbor interaction only, with a spring constant of k. By introducing indices β and γ to denote the nearest neighboring atoms of atom α, the specific terms in Eqs.(8) and (9) are given as

$$\mathbb{K}_{kin}=-\int_{I_n}\left(\sum_{\alpha=1}^{N_a}m_\alpha\dot{\mathbf{N}}_\alpha^T\ddot{\mathbf{N}}_\alpha\right)dt \qquad (10)$$

$$\mathbb{K}_{int}=\int_{I_n}\sum_{\alpha=1}^{N_a}\frac{k}{2}\left(\dot{\mathbf{N}}_\alpha^T\mathbb{N}_\alpha+\dot{\mathbf{N}}_\beta^T\mathbb{N}_\beta+\dot{\mathbf{N}}_\gamma^T\mathbb{N}_\gamma\right)dt \qquad (11)$$

$$\mathbb{K}_{kin}^+=-\sum_{\alpha=1}^{N_a}m_\alpha\left(\dot{\mathbf{N}}_\alpha^T(t_n^+)\dot{\mathbf{N}}_\alpha(t_n^+)\right) \qquad (12)$$

$$
\begin{aligned}
\mathbb{K}_{int}^+=\sum_{\alpha=1}^{N_a}\frac{k}{2}\Big(&\mathbf{N}_\alpha^T(t_n^+)\mathbb{N}_\alpha(t_n^+)+\mathbf{N}_\beta^T(t_n^+)\mathbb{N}_\beta(t_n^+) \\
&+\mathbf{N}_\gamma^T(t_n^+)\mathbb{N}_\gamma(t_n^+)\Big) \qquad (13)
\end{aligned}
$$

$$\mathbb{L}_{kin}^-=-\sum_{\alpha=1}^{N_a}m_\alpha\left(\dot{\mathbf{N}}_\alpha^T(t_n^+)\dot{\mathbf{N}}_\alpha(t_n^-)\right) \qquad (14)$$

$$
\begin{aligned}
\mathbb{L}_{int}^-=\sum_{\alpha=1}^{N_a}\frac{k}{2}\Big(&\mathbf{N}_\alpha^T(t_n^+)\mathbb{N}_\alpha(t_n^-)+\mathbf{N}_\beta^T(t_n^+)\mathbb{N}_\beta(t_n^-) \\
&+\mathbf{N}_\gamma^T(t_n^+)\mathbb{N}_\gamma(t_n^-)\Big) \qquad (15)
\end{aligned}
$$

$$
\begin{aligned}
(\mathbb{L}_{ext})_n=&-\int_{I_n}\left(\sum_{\alpha=1}^{N_a}\dot{\mathbf{N}}_\alpha^T\mathbf{f}_\alpha^{ext}\right)dt \\
&-\sum_{\alpha=1}^{N_a}\mathbf{N}_\alpha(t_n^+)\cdot\left[\!\!\left[\mathbf{f}_\alpha^{ext}\right]\!\!\right]_{t=t_n} \qquad (16)
\end{aligned}
$$

where

$$\mathbf{N}_\alpha=\mathbf{N}(\mathbf{x}_\alpha,t),\mathbf{N}_\beta=\mathbf{N}(\mathbf{x}_\beta,t),\mathbf{N}_\gamma=\mathbf{N}(\mathbf{x}_\gamma,t) \qquad (17)$$

$$\mathbb{N}_\alpha=\mathbf{N}_\beta+\mathbf{N}_\gamma-2\mathbf{N}_\alpha \qquad (18)$$

$$\mathbb{N}_\beta=\mathbf{N}_\alpha-\mathbf{N}_\beta \qquad (19)$$

$$\mathbb{N}_\gamma=\mathbf{N}_\alpha-\mathbf{N}_\gamma \qquad (20)$$

In numerical implementation, the evaluation of the terms in Eqs.(8) and (9) can be further simplified using the virtual atom cluster (VAC) model

developed in (Qian, Wagner, and Liu (2004) and Qian and Gondhalekar (2004)). In this model, the original discrete summation over the atoms is replaced by quadrature. At each quadrature point, a basic repeating unit of virtual atom cluster is imposed and the potential energy density and its dependence on the deformation mapping are evaluated based on the cluster representation. For the $1D$ chain of atoms with nearest neighbor interaction only, the virtual atom cluster consists of 3 atoms, α being the atom imposed on the quadrature point, β its neighbor to the left and γ its neighbor to the right. The corresponding terms in the space-time FEM equation further reduce to:

$$\mathbb{K}_{kin} = -\int_{I_n} \rho_m \left(\sum_{g=1}^{n_g} \dot{\mathbf{N}}_\alpha^T \ddot{\mathbf{N}}_\alpha \, |J_x| \, w_g \right) dt \tag{21}$$

$$\mathbb{K}_{int} = \int_{I_n} \rho_k \left(\sum_{g=1}^{n_g} \left(\dot{\mathbf{N}}_\alpha^T \mathbb{N}_\alpha + \dot{\mathbf{N}}_\beta^T \mathbb{N}_\beta + \dot{\mathbf{N}}_\gamma^T \mathbb{N}_\gamma \right) |J_x| w_g \right) dt \tag{22}$$

$$\mathbb{K}_{kin}^{+} = -\rho_m \sum_{g=1}^{n_g} \left(\dot{\mathbf{N}}_\alpha^T(t_n^+) \dot{\mathbf{N}}_\alpha(t_n^+) \right) |J_x| \, w_g \tag{23}$$

$$\mathbb{K}_{int}^{+} = \rho_k \sum_{g=1}^{n_g} \left(\mathbf{N}_\alpha^T(t_n^+) \mathbb{N}_\alpha(t_n^+) + \mathbf{N}_\beta^T(t_n^+) \mathbb{N}_\beta(t_n^+) + \mathbf{N}_\gamma^T(t_n^+) \mathbb{N}_\gamma(t_n^+) \right) |J_x| w_g \tag{24}$$

$$\mathbb{L}_{kin}^{-} = -\rho_m \sum_{g=1}^{n_g} \left(\dot{\mathbf{N}}_\alpha^T(t_n^+) \dot{\mathbf{N}}_\alpha(t_n^-) \right) |J_x| \, w_g \tag{25}$$

$$\mathbb{L}_{int}^{-} = \rho_k \sum_{g=1}^{n_g} \left(\mathbf{N}_\alpha^T(t_n^+) \mathbb{N}_\alpha(t_n^-) + \mathbf{N}_\beta^T(t_n^+) \mathbb{N}_\beta(t_n^-) + \mathbf{N}_\gamma^T(t_n^+) \mathbb{N}_\gamma(t_n^-) \right) |J_x| w_g \tag{26}$$

where

$$\rho_m = \frac{m_\alpha}{h_a} \tag{27}$$

$$\rho_k = \frac{k}{2h_a} \tag{28}$$

in which n_g are the number of quadrature points, w_g are the quadrature weights, J_x represents the Jacobian for the spatial quadrature and h_a is the inter-atomic spacing.

2.2 Space-time FEM without Enrichment

In this section, we first compare the performances of the space-time FEM approach developed in the last section with the standard molecular dynamics. We consider a 1D chain of atoms which is fixed at both ends. The two ends are located at $x = -1$ and $x = 1$. The number of atoms in this chain is 1001. Thus the atomic spacing h_a is 0.002. The mass of each atom $m_\alpha = 1$ and the value of k for the harmonic potential between the neighboring atoms is 2. For the space-time simulation, the spatial discretization is done by placing a spatial node at each of the atomic location. Therefore the total number of spatial nodes is the same as the total number of atoms, i.e. $n_c = N_a = 1001$ and the nodal spacing $h_e = h_a = 0.002$. Quadratic interpolation in time is used. An initial displacement of $A = \frac{2h_a}{3}$ is applied to atoms in the region from $x = \pm L_c$ and $L_c = 0.2$.

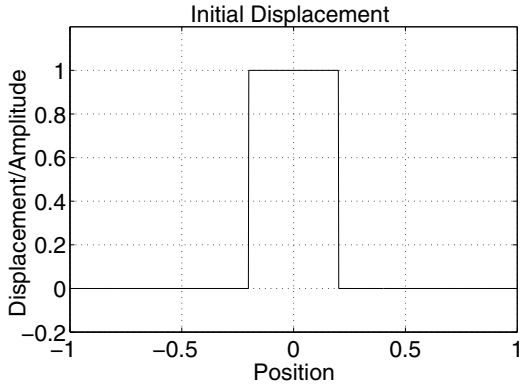

Figure 2: Initial step wave profile for the space-time FEM simulation

Shown in Figure 2 is the initial imposed wave profile. The time history of the wave is simulated using both MD and space-time methods. The standard Verlet algorithm is employed in the MD simulation and the time step used is $\delta t = 0.96\sqrt{\frac{m_a}{k}}$. In the space-time method, we have employed two different time step sizes, i.e., Δt is 5 times that of MD in the first case and 10 times for the second case.

Figures 3 and 4 shows the positions of the atoms resolved from MD and space-time method at the end of 200 MD steps. The analytical solution is

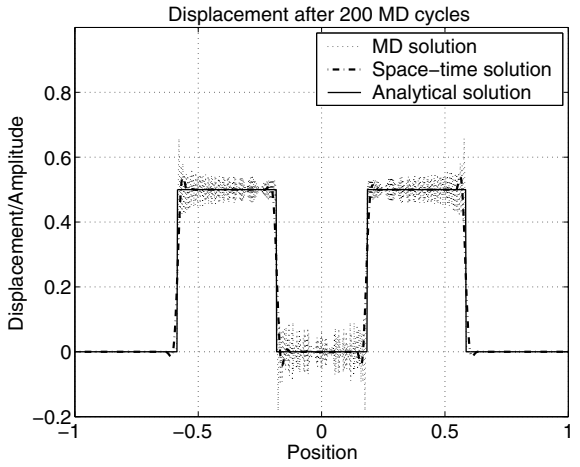

Figure 3: Comparison of space-time FEM solutions with analytical and MD solutions at $\Delta t = 5\delta t$

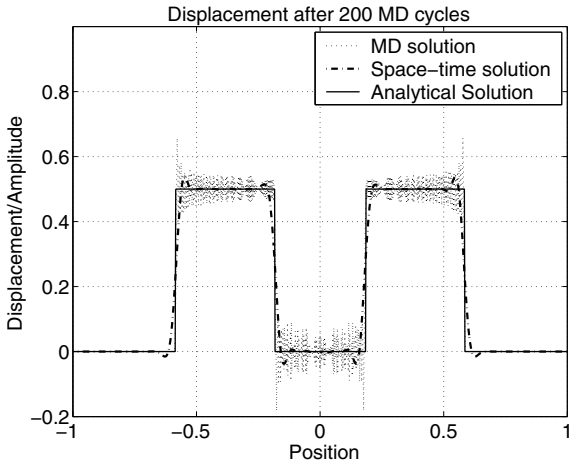

Figure 4: Comparison of space-time FEM solutions with analytical and MD solutions at $\Delta t = 10\delta t$

also plotted for reference. As can be seen from figures 3 and 4, the space-time method produces far less oscillations compared with the MD solution and the jump in the displacement is well captured. Figure 4 indicates that the space-time solution remains stable even with the use of a larger time step ($\Delta t = 10\delta t$), though there is some minor reduction in accuracy in the vicinity of the region where the jump in the displacement of the atoms takes place.

Since the space-time approximation in this example is established using the regular FEM shape functions, the coarse scale approximation based on FEM could be problematic if one attempts to couple it with atomistic simulations. A similar issue has been discussed in (Wagner and Liu (2003)) in the context of semi-discrete scheme. Here we demonstrate the mismatch effects in the context of coupling space-time FEM with MD. In this approach the MD is limited to certain regions of interest. We consider the same mass and spring constant as in the last example and the domain now extends from $x = -L$ to $x = L$ with 4001 atoms and $L = 2$. The spatial domain is discretized using 161 nodes. The atomic spacing is thus $h_a = 0.001$ and the space-time FEM spatial nodal spacing is $h_e = 0.025$. The FEM description exists everywhere in the domain including the regions where MD is applied. In this example, the MD description is limited to two regions. The first MD region stretches between $x = \pm\frac{3L}{16}$ and is referred to as the central MD region. The second region extends from $x = 0.3L$ to $x = 0.6L$ and is called peripheral MD region. We first implement a handshake approach for the coupling of the space-time FEM with MD. This is schematically illustrated in Figure 5. In this approach,

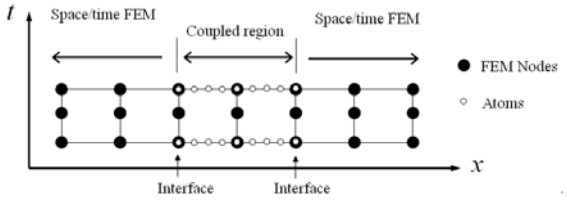

Figure 5: Coupling space-time FEM with molecular dynamics using handshake approach

the handshake coupling is mainly implemented through the so-called 'ghost atoms'. By definition, these are the atoms located just outside the interfacial boundary of the MD-FEM region i.e. they lie in the FEM region. The displacement for these atoms is interpolated from the space-time FEM and it is supplied as boundary condition for the MD simulation. In addition, for the atoms in the MD regions that are located on the MD-FEM

interfacial boundary, we also enforce the velocities of these atoms to be interpolated from the space-time FEM method. This is also referred to as the velocity matching condition in (Wagner and Liu (2003)). To take advantage of the large time step that can be used in the space-time FEM, the coarse scale time step for the coupled space-time/MD simulation is $\Delta t = 600\delta t$, where $\delta t = 0.1\sqrt{\frac{k}{m_a}}$ is the MD time step.

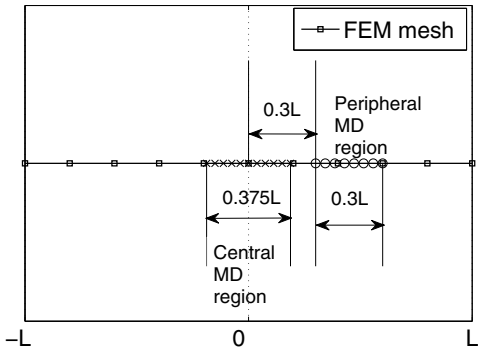

Figure 6: Spatial discretization scheme of coupling MD with space-time FEM

Figure 6 is a schematic description for the spatial discretization of the domain. The initial displacement is applied in the region extending from $x = -L_c$ to $x = L_c$, where $L_c = L/10$. The form

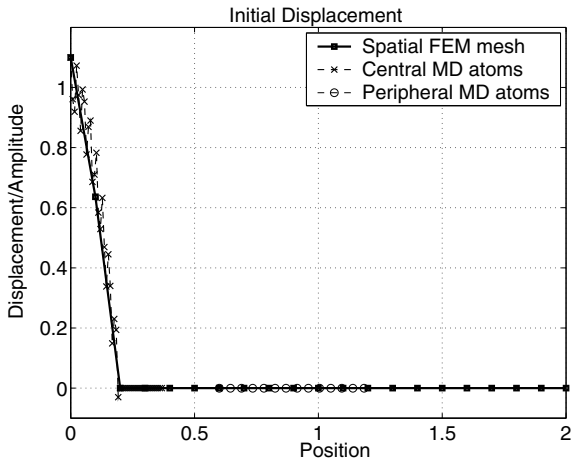

Figure 7: Initial displacement in the coupled space-time FEM/MD simulation

of the initial displacement contains a combination of coarse plus fine scale wave, which is given as follows:

$$\mathbf{u} = \begin{cases} 0 & \text{if } |\, x \,| > L_c \\ A\left[\cos\left(\frac{\pi x}{2L_c}\right) + 0.1\cos\left(\frac{B\pi x}{2L_c}\right)\right] & \text{if } |\, x \,| \le L_c \end{cases} \tag{29}$$

where $A = \frac{2h_a}{3}$ and B is a parameter that controls the fine scale portion of the displacement. For the results that are presented over here, the parameter $B = 69$.

The initial displacement is plotted in Figure 7 only for the positive half of the domain due to symmetry. As we observe from Figure 7, only the atoms in the first MD region are subjected to the prescribed displacement, while those in the second MD region are initially at rest. As the simulation proceeds, the initial coarse plus fine scale displacement field shall pass through the central atoms and propagate into the second MD region according to the analytical solution.

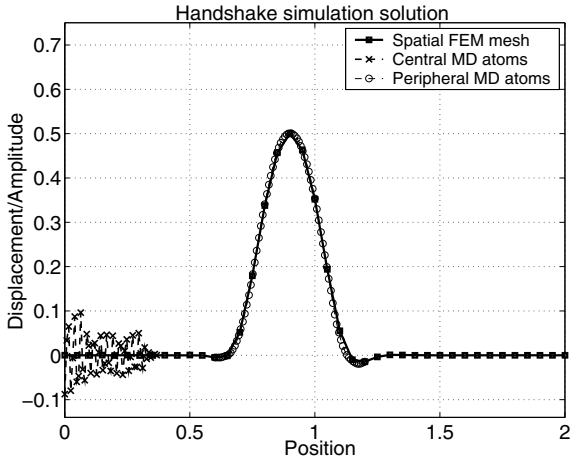

Figure 8: Spurious wave reflection from the direct handshake approach at 9000 MD step

In the coupled simulation based on the direct handshake approach, however, only the coarse scale portion of the imposed displacement passes through the interface while the fine scale portion gets reflected. This can be clearly identified from the displacement field for the atoms located in the central MD region in Figure 8. Note that only positive half of the domain is plotted in Figure 8 due

to the symmetry of the solution. The observed spurious reflection is mainly due to the mismatch in the FEM mesh size and atomic spacing. A more quantitative evaluation of the reflection is to compute the total energy of the atoms in the two MD regions. The total energy is calculated by considering the kinetic as well as the internal energy of all the atoms in the corresponding MD regions. Figure 9 plots the energy histories for the central and peripheral MD regions based on the handshake coupling approach. For comparison purpose, the corresponding energy histories from the full-scale MD simulation are also computed and plotted in Figure 9. All the energy values are normalized with respect to the initial energy. We observe from Figure 9 that over 60%

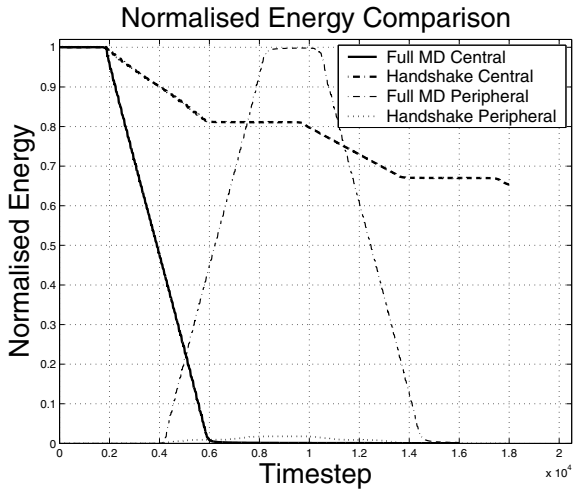

Figure 9: A comparison of normalized energy history from the handshake case with the full-scale MD simulation

of the energy is reflected at the interface and retained in the first MD region. The second MD region gets only a small fraction (<2%) of the total energy. This energy mainly corresponds to the coarse scale portion of the displacement that gets transmitted through the FEM region into the peripheral MD region. One could further perform a parametric study by changing the value of B as it controls the fine scale feature of the imposed displacement. As B increases, the ratio of the energy transmitted into 2nd MD region to the total initial energy decreases. In other words, with the increase in the fineness of the fine scale component, the amount of the spurious reflection increases and the peripheral region receives smaller portion of the total energy. Figure 10 quantitatively shows this dependence. To eliminate the interface reflec-

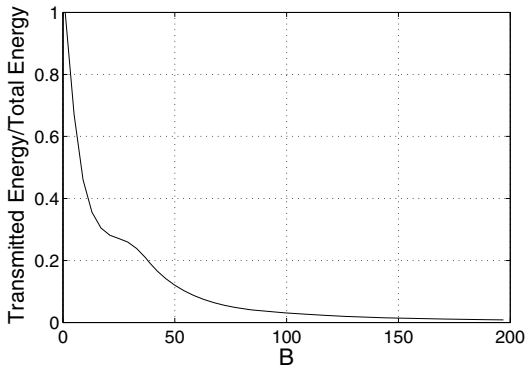

Figure 10: The ratio of transmitted energy vs total energy as a function of the parameter B

tion, we have applied the technique of Bridging Scale Method (BSM) (Wagner and Liu (2003)). The readers are referred to the reference (Wagner and Liu (2003)) for the details. The implementation in this paper follows a similar procedure, with the exception that the FEM solutions are obtained from the space-time framework instead of semi-discrete scheme. Here we plot in Figure 11

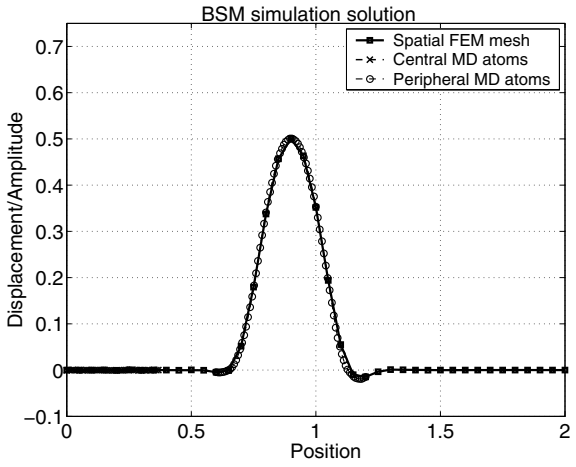

Figure 11: Displacement plot indicating elimination of reflection

for the wave profile at the same time as Figure

8 after BSM is applied. We observe that the reflections are effectively eliminated. However, we also observe that only the coarse scale portion of the displacement is propagated into the peripheral region through the FEM region. Figure 12 illustrates that the energy associated with the fine scale is dissipated and thus no longer retained in the central MD region. Compared with the solution for the peripheral MD region based on full-scale MD, one clearly sees that the total energy is not conserved. This phenomenon is mainly due to the lack of fine scale representation in the space-time FEM approximation.

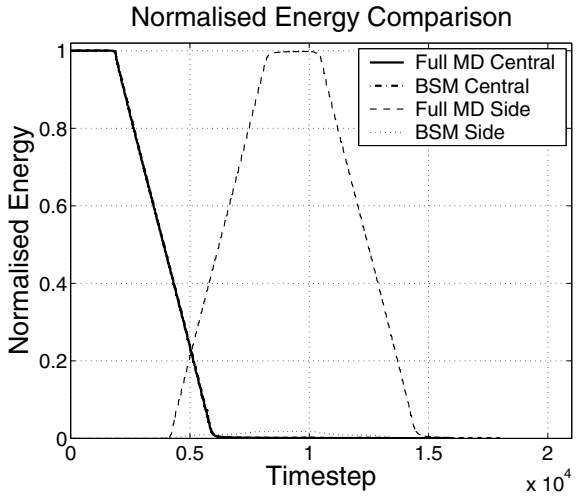

Figure 12: Normalized energy plot for the BSM simulation

3 Extended Space-time Finite Element Method based on Multiscale Enrichment

The discussions in the previous section clearly illustrate the need for introducing multiscale space-time approximations into the regular space-time FEM. In this paper we have developed an enrichment method based on a new generation of numerical approach called extended finite element method (XFEM) (Dolbow, Moes, and Belytschko (2000a,b); Sukumar, Moes, Moran, and Belytschko (2000); Chessa and Belytschko (2004)), which is also sometimes referred to as the Generalized FEM (GFEM) (Duarte, Babuška, and Oden (2000)). Both methods are derived based on the partition-of-unity approach introduced in (Melenk and Babuška (1996)).

We start describing the enrichment formulation by defining $\phi(\mathbf{x},t)$ as a function that represents certain fine scale physics in both space and time. In the enriched formulation we multiply the regular FEM shape function defined at the node J with $(\phi(\mathbf{x},t)-\phi(\mathbf{x}_J,t_J))$ to obtain the enriched basis, where $(\mathbf{x}_J,t_J)$ is the space-time coordinate of node J. The total displacement at any point in space and time is given as:

$$\mathbf{u}=\sum_{I=1}^{n}\overline{N}_I(\mathbf{x},t)\,\overline{d}_I+\sum_{J=1}^{n_e}\tilde{N}_J(\mathbf{x},t)\,a_J \tag{30}$$

where n_e is the number of enriched nodes and it is a subset of the total number of space-time nodes n. a_J are the additional degrees of freedom at the enriched nodes. $\overline{N}_I$ represents the regular space-time FEM shape function with the corresponding nodal degree of freedom $\overline{d}_I$, while $\tilde{N}_J$ represents the enrichment shape function. The enrichment shape function $\tilde{N}_J(\mathbf{x},t)$ is given by:

$$\tilde{N}_J(\mathbf{x},t)=\overline{N}_J(\mathbf{x},t)\cdot\psi(\mathbf{x},t) \tag{31}$$

where,

$$\psi(\mathbf{x},t)=(\phi(\mathbf{x},t)-\phi(\mathbf{x}_J,t_J)) \tag{32}$$

The definition of $\psi(\mathbf{x},t)$ in Eq.(32) ensures that the nodal values $\overline{d}_I$ at the node I equals the displacement evaluated at the corresponding node.

In a time dependent problem, the local character changes with time and the domains that need to be enriched are constantly changing. As a result, the enrichment function at a particular location in space can be different at different times. For the 1D implementation in this paper, the enrichment degrees of freedom are present in the entire domain. This reduces the need of tracking the local character, but the trade-off is the increase in the number of degrees of freedom that we solve. We expect, however, future improvement can be made by using an enrichment scheme that is limited to the region of the local character. Let $\mathbf{N}$ represent the total shape function matrix, $\mathbf{N}=[\overline{\mathbf{N}}\quad\tilde{\mathbf{N}}]$. The displacement can be obtained by:

$$\mathbf{u}=\overline{\mathbf{N}}\,\overline{\mathbf{d}}+\tilde{\mathbf{N}}\,\mathbf{a}=\mathbf{N}\,\mathbf{d} \tag{33}$$

where $\mathbf{d} = [\overline{\mathbf{d}}, \mathbf{a}]^T$.

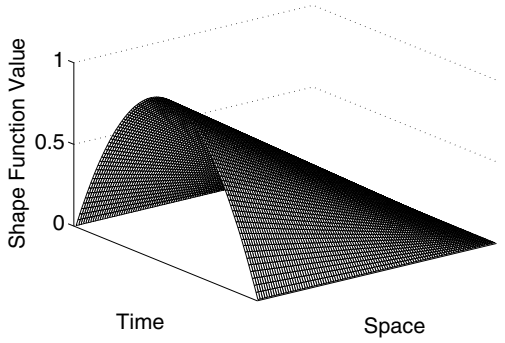

Figure 13: Regular FEM shape function

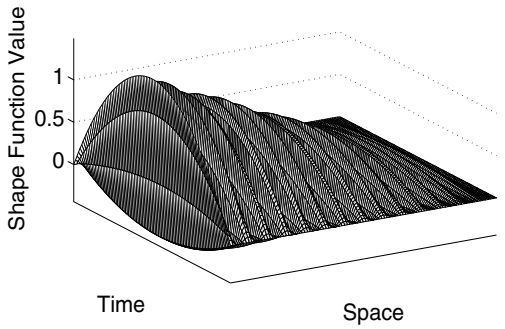

Figure 14: Enrichment FEM shape function

Figures 13 and 14 shows the regular FEM shape function $\overline{\mathbf{N}}$ and the enrichment shape function $\tilde{\mathbf{N}}$ for a single space-time finite element. In this case, the three-node quadratic function is used for interpolation in time and linear function is used in space for the regular FEM shape function. A harmonic cosine function corresponding to the fine scale portion of the displacement from Eq.(29), with $B = 69$ is used as the enrichment function . As mentioned earlier, the effect of enrichment on the shape function basis is expected to vanish at the corresponding enriched node. The multiscale approximation constructed from Eq.(33) is similar in form to the approximation in a regular FEM, with the exception of enrichment basis. For a linear lattice, a stiffness equation in the same form as Eq.(7) can be derived

$$\mathbb{K}_n \mathbf{d}_{n+1} = \mathbb{L}_n \mathbf{d}_n + (\mathbb{L}_{ext})_n \tag{34}$$

where

$$\mathbb{K}_n = \mathbb{K}_{kin} + \mathbb{K}_{int} + \mathbb{K}^+_{kin} + \mathbb{K}^+_{int} \tag{35}$$

$$\mathbb{L}_n = \mathbb{L}^-_{kin} + \mathbb{L}^-_{int} \tag{36}$$

and the specific terms are given as

$$\mathbb{K}_{kin} = -\int_{I_n} \rho_m \sum_{g=1}^{n_g} \begin{bmatrix} \dot{\overline{\mathbf{N}}}^T_\alpha \\ (\dot{\tilde{\mathbf{N}}}_\alpha)^T_n \end{bmatrix} \begin{bmatrix} \ddot{\overline{\mathbf{N}}}_\alpha & (\ddot{\tilde{\mathbf{N}}}_\alpha)_n \end{bmatrix} |J_x| w_g \, dt \tag{37}$$

$$\mathbb{K}_{int} = \int_{I_n} \rho_k \sum_{g=1}^{n_g} \Bigg(\begin{bmatrix} \dot{\overline{\mathbf{N}}}^T_\alpha \\ (\dot{\tilde{\mathbf{N}}}_\alpha)^T_n \end{bmatrix} \begin{bmatrix} \overline{\mathbb{N}}_\alpha & (\tilde{\mathbb{N}}_\alpha)_n \end{bmatrix} + \begin{bmatrix} \dot{\overline{\mathbf{N}}}^T_\beta \\ (\dot{\tilde{\mathbf{N}}}_\beta)^T_n \end{bmatrix} \begin{bmatrix} \overline{\mathbb{N}}_\beta & (\tilde{\mathbb{N}}_\beta)_n \end{bmatrix} + \begin{bmatrix} \dot{\overline{\mathbf{N}}}^T_\gamma \\ (\dot{\tilde{\mathbf{N}}}_\gamma)^T_n \end{bmatrix} \begin{bmatrix} \overline{\mathbb{N}}_\gamma & (\tilde{\mathbb{N}}_\gamma)_n \end{bmatrix} \Bigg) |J_x| w_g \, dt \tag{38}$$

$$\mathbb{K}^+_{kin} = -\rho_m \Bigg(\sum_{g=1}^{n_g} \begin{bmatrix} \dot{\overline{\mathbf{N}}}^T_\alpha(t_n^+) \\ (\dot{\tilde{\mathbf{N}}}_\alpha)^T_n(t_n^+) \end{bmatrix} \left[\dot{\overline{\mathbf{N}}}_\alpha(t_n^+) \; (\dot{\tilde{\mathbf{N}}}_\alpha)_n(t_n^+) \right] |J_x| w_g \Bigg) \tag{39}$$

$$\mathbb{K}^+_{int} = \rho_k \sum_{g=1}^{n_g} \Bigg(\begin{bmatrix} \overline{\mathbf{N}}^T_\alpha(t_n^+) \\ (\tilde{\mathbf{N}}_\alpha)^T_n(t_n^+) \end{bmatrix} \begin{bmatrix} \overline{\mathbb{N}}_\alpha(t_n^+) & (\tilde{\mathbb{N}}_\alpha)_n(t_n^+) \end{bmatrix} + \begin{bmatrix} \overline{\mathbf{N}}^T_\beta(t_n^+) \\ (\tilde{\mathbf{N}}_\beta)^T_n(t_n^+) \end{bmatrix} \begin{bmatrix} \overline{\mathbb{N}}_\beta(t_n^+) & (\tilde{\mathbb{N}}_\beta)_n(t_n^+) \end{bmatrix} + \begin{bmatrix} \overline{\mathbf{N}}^T_\gamma(t_n^+) \\ (\tilde{\mathbf{N}}_\gamma)^T_n(t_n^+) \end{bmatrix} \begin{bmatrix} \overline{\mathbb{N}}_\gamma(t_n^+) & (\tilde{\mathbb{N}}_\gamma)_n(t_n^+) \end{bmatrix} \Bigg) |J_x| w_g \tag{40}$$

$$\mathbb{L}^-_{kin} = -\rho_m \sum_{g=1}^{n_g} \begin{bmatrix} \dot{\overline{\mathbf{N}}}^T_\alpha(t_n^+) \\ (\dot{\tilde{\mathbf{N}}}_\alpha)^T_n(t_n^+) \end{bmatrix} \begin{bmatrix} \dot{\overline{\mathbf{N}}}_\alpha(t_n^-) & (\dot{\tilde{\mathbf{N}}}_\alpha)_n(t_n^-) \end{bmatrix} |J_x| w_g \tag{41}$$

$$\mathbb{L}_{int}^{-} = \rho_k \sum_{g=1}^{n_g} \left(\begin{bmatrix} \overline{\mathbf{N}}_\alpha^T(t_n^+) \\ (\tilde{\mathbf{N}}_\alpha)_n^T(t_n^+) \end{bmatrix} \begin{bmatrix} \overline{\mathbb{N}}_\alpha(t_n^-) & (\tilde{\mathbb{N}}_\alpha)_n(t_n^-) \end{bmatrix} + \begin{bmatrix} \overline{\mathbf{N}}_\beta^T(t_n^+) \\ (\tilde{\mathbf{N}}_\beta)_n^T(t_n^+) \end{bmatrix} \begin{bmatrix} \overline{\mathbb{N}}_\beta(t_n^-) & (\tilde{\mathbb{N}}_\beta)_n(t_n^-) \end{bmatrix} + \begin{bmatrix} \overline{\mathbf{N}}_\gamma^T(t_n^+) \\ (\tilde{\mathbf{N}}_\gamma)_n^T(t_n^+) \end{bmatrix} \begin{bmatrix} \overline{\mathbb{N}}_\gamma(t_n^-) & (\tilde{\mathbb{N}}_\gamma)_n(t_n^-) \end{bmatrix} \right) |J_x| w_g \tag{42}$$

$$(\mathbb{L}_{ext})_n = -\int_{I_n} \sum_{\alpha=1}^{N_a} \begin{bmatrix} \dot{\overline{\mathbf{N}}}_\alpha^T \\ (\dot{\tilde{\mathbf{N}}}_\alpha)_n^T \end{bmatrix} \mathbf{f}_\alpha^{ext}\, dt - \sum_{\alpha=1}^{N_a} \begin{bmatrix} \overline{\mathbf{N}}_\alpha^T(t_n^+) \\ (\tilde{\mathbf{N}}_\alpha)_n^T(t_n^+) \end{bmatrix} [\![\mathbf{f}_\alpha^{ext}]\!]_{t=t_n} \tag{43}$$

Eq.(34) represents the equation that we solve in the extended space-time finite elements to obtain $\mathbf{d_{n+1}}$ from the knowledge of $\mathbf{d_n}$. This general form is independent of the choice for the enrichment function. Note that the enrichment shape function $\tilde{\mathbf{N}}$ is a function of time and therefore a subscript n is used. Depending upon the problem under analysis $\phi(\mathbf{x},t)$ will change resulting in a different $\tilde{\mathbf{N}}$ matrix for different problems. This will obviously impact the final form for $\mathbb{K}_n$ and $\mathbb{L}_n$ that would be used to program the enriched space time finite element formulation. This choice is further discussed in the case of coupling the extended space-time FEM with molecular dynamics to be presented in the next section.

4 Coupling of the Extended Space-time FEM with Molecular Dynamics

The coupling scheme in the enriched case is similar to the case of coupling the regular space-time FEM with MD, i.e., the space-time FEM spans the entire domain and the MD is limited to only a portion of the domain. As MD typically employs an explicit time integration scheme with small time step size, we will develop a multi-time stepping algorithm. In this algorithm, the coarse scale simulation associated with the space-time FEM is advanced first. For every coarse scale time step, m sub-cycles are carried out for the MD simulation. In the following description, we use superscript j for the time step number of the MD sub-cycle and n for the time step number of the extended space-time FEM simulation. The specific implementations for the MD and space-time FEM are described in the following sections.

4.1 MD Solution Procedure

Let $\mathbf{q}$ represent the atomic displacement vector and $\mathbf{M_A}$ be the atomic mass matrix for the local MD region, the governing equation of MD is given as

$$\mathbf{M_A}\ddot{\mathbf{q}} = \mathbf{f_{int}} + \mathbf{f_{ext}} \tag{44}$$

where $\mathbf{f_{int}} = -\frac{\partial W}{\partial \mathbf{q}}$ is the internal force, W is the interatomic potential and $\mathbf{f_{ext}}$ is the external force vector.

For the j-th sub-cycle within the n-th space-time FEM time step, we define $\mathbf{q}_n^j$, $\mathbf{p}_n^j$ and $\ddot{\mathbf{q}}_n^j$ as the corresponding MD displacement, momentum and acceleration vectors. To proceed with the MD simulation sub-cycle $j+1$, boundary conditions shall be specified based on the extended space-time FEM simulation. Denote $\Gamma_{FE/MD}$ as the interfacial boundary where the ghost atoms are located, the boundary condition for the MD sub-cycle is given as

$$\mathbf{q}_n^{j+1}|_{\Gamma_{FE/MD}} = \mathbf{q}(\mathbf{x}, t_n^{j+1})|_{\Gamma_{FE/MD}} = \mathbf{N}(\mathbf{x}, t_n^{j+1})\mathbf{d}|_{\Gamma_{FE/MD}} \tag{45}$$

in which t_n^{j+1} stands for the time corresponding to the $(j+1)$-th sub-cycle of the n-th step. With Eq.(45), the Verlet algorithm is used to advance the MD simulation:

$$\mathbf{q}_n^{j+1} = \mathbf{q}_n^j + \delta t\, \mathbf{M}_\mathbf{A}^{-1}\, \dot{\mathbf{p}}_n^j + \frac{1}{2}\, \delta t^2\, \ddot{\mathbf{q}}_n^j \tag{46}$$

$$\ddot{\mathbf{q}}_n^{j+1} = \mathbf{M}_\mathbf{A}^{-1}\, \mathbf{f}(\mathbf{q}_n^{j+1}, \mathbf{q}_n^{j+1}|_{\Gamma_{FE/MD}}, \theta) \tag{47}$$

$$\mathbf{p}_n^{j+1} = \mathbf{p}_n^j + \frac{1}{2}\mathbf{M_A}\, \delta t\, (\ddot{\mathbf{q}}_n^{j+1} + \ddot{\mathbf{q}}_n^j) \tag{48}$$

in which θ represents the time history kernel (Wagner and Liu (2003)) that is evaluated for the

atoms at the boundaries of MD, δt is the time step size used for the sub-cycle. The set of equations (Eq.(45)-(48)) are used to update the MD simulation. As can be seen, the boundary information for the MD simulation is obtained from the space-time FEM simulation using the same handshake approach as described in section 2. The key difference, however, is that the positions of the ghost atoms are interpolated based on the extended space-time FEM approximation. In addition, we no longer implement the velocity matching condition.

4.2 Extended Space-time FEM Simulation

In the implementation of the extended space-time FEM, Eq.(34) is solved to advance the coarse scale simulation with a much larger time step size. In the regions where the space-time mesh overlaps with the MD, the handshake approach described in the last section represents the information passing from the extended space-time FEM to MD. In addition, we note that the total scale solution obtained from MD in this region is readily available. Therefore, the space-time FEM solution in the overlap region can be obtained by projecting the MD solution onto the extended space-time FEM shape function basis. This in turn represents the information passing from MD to the extended space-time FEM.

We define n_a as the number of atoms in the coupled region and n_{ac} as the number of spatial nodes in the coupled region. If the atomistic DOFs in the coupled region are directly interpolated using the extended space-time FEM shape functions, we have

$$\hat{\mathbf{q}}(\mathbf{x},t) = \hat{\mathbf{N}}(\mathbf{x},t)\mathbf{D} \tag{49}$$

in which $\hat{\mathbf{q}}$ is the atomistic DOF in the coupled region that is interpolated from the space-time shape function matrix $\hat{\mathbf{N}}(\mathbf{x},t)$ that contains both the regular and enrichment shape functions for the atoms in the coupled region. The nodal DOF $\mathbf{D}$ are defined in the same coupled region. The projection operator is obtained by minimizing the difference e between the MD solution $\mathbf{q}$ and the interpolated value $\hat{\mathbf{q}}$ in a weighted least-square sense (Wagner and Liu (2003)). This error is expressed as

$$e = (\mathbf{q}-\hat{\mathbf{q}})^{\mathbf{T}}\mathbf{M_A}(\mathbf{q}-\hat{\mathbf{q}}) \tag{50}$$

$\mathbf{M_A}$ is diagonal mass matrix corresponding to the atoms in the coupled region. Considering the multiscale approximation in Eq.(49), the minimization of e yields

$$\hat{\mathbf{N}}\mathbf{D} = \hat{\mathbf{N}}(\hat{\mathbf{N}}^{\mathbf{T}}\mathbf{M_A}\hat{\mathbf{N}})^{-\mathbf{1}}\hat{\mathbf{N}}^{\mathbf{T}}\mathbf{M_A}\mathbf{q} = \mathbf{P}\mathbf{q} \tag{51}$$

in which we defined the projection operator $\mathbf{P} = \hat{\mathbf{N}}(\hat{\mathbf{N}}^{\mathbf{T}}\mathbf{M_A}\hat{\mathbf{N}})^{-\mathbf{1}}\hat{\mathbf{N}}^{\mathbf{T}}\mathbf{M_A}$. This in turn gives

$$\mathbf{D} = (\hat{\mathbf{N}}^{\mathbf{T}}\mathbf{M_A}\hat{\mathbf{N}})^{-\mathbf{1}}\hat{\mathbf{N}}^{\mathbf{T}}\mathbf{M_A}\mathbf{q} \tag{52}$$

which is used to update the extended space-time nodal DOFs.

In computational implementation, a multiplicative form is adopted for the extended space-time FEM shape function, expressed as

$$\begin{aligned}\hat{\mathbf{N}}(\mathbf{x},t) = [&N_{t1}\mathbf{N_x} \quad N_{t2}\mathbf{N_x} \quad N_{t3}\mathbf{N_x} \\ &N_{t1}\mathbf{N_x}\psi(\mathbf{x},t) \quad N_{t2}\mathbf{N_x}\psi(\mathbf{x},t) \quad N_{t3}\mathbf{N_x}\psi(\mathbf{x},t)]\end{aligned} \tag{53}$$

In Eq.(53) we have used quadratic interpolation in time and linear interpolation in space. Here N_{t1}, N_{t2} and N_{t3} are the time shape functions defined at t_n, $t_{n+1/2}$ and t_{n+1}, respectively. $\mathbf{N_x}$ gives the linear shape function in space. As a result of the interpolation using Eq.(53), the enriched shape function matrix $\hat{\mathbf{N}}(\mathbf{x},t)$ will be of size $(n_a \times 6n_{ac})$. The nodal DOF in the coupled region $\mathbf{D}$ is given as

$$\mathbf{D} = [\overline{\mathbf{D}}_n \quad \overline{\mathbf{D}}_{n+1/2} \quad \overline{\mathbf{D}}_{n+1} \quad \tilde{\mathbf{D}}_n \quad \tilde{\mathbf{D}}_{n+1/2} \quad \tilde{\mathbf{D}}_{n+1}]^T \tag{54}$$

in which $\overline{\mathbf{D}}$ and $\tilde{\mathbf{D}}$ represent the regular and enriched DOFs defined at the space-time nodes. Subscripts n, $n+1/2$ and $n+1$ correspond to the time at t_n, $t_{n+1/2}$ and t_{n+1}, respectively. The projection operation is performed at time $t_{n+1/2}$ and t_{n+1}. At time $t_{n+1/2}$, the shape function matrix reduces to:

$$\begin{aligned}\hat{\mathbf{N}}(\mathbf{x},t=t_{n+1/2}) = \\ \begin{bmatrix}\mathbf{0} & \mathbf{N_x} & \mathbf{0} & \mathbf{0} & \mathbf{N_x}\psi(\mathbf{x},t_{n+1/2}) & \mathbf{0}\end{bmatrix}\end{aligned} \tag{55}$$

Thus we could define a simplified shape function matrix $\mathbf{N_s}^{t_{n+1/2}} = [\mathbf{N_x} \quad \mathbf{N_x}\psi(\mathbf{x}, t_{n+1/2})]$ at time $t_{n+1/2}$. Similarly, at time t_{n+1} we have $\mathbf{N_s}^{t_{n+1}} = [\mathbf{N_x} \quad \mathbf{N_x}\psi(\mathbf{x}, t_{n+1})]$. Let $\mathbf{q}_n^{m/2}$ be the MD solution after $m/2$ sub-steps and $\mathbf{q}_n^m$ be the MD solution after m sub-steps for the j-th space-time FEM time step. Based on the projection operator defined from Eq.(51), we have for the m-th sub-cycle,

$$[\overline{\mathbf{D}}_{n+1} \quad \tilde{\mathbf{D}}_{n+1}]^T = \left[(\mathbf{N_s}^{t_{n+1}})^T \mathbf{M_A} \mathbf{N_s}^{t_{n+1}}\right]^{-1} (\mathbf{N_s}^{t_{n+1}})^T \mathbf{M_A} \mathbf{q}_n^m \quad (56)$$

Similarly at the half step, the space-time DOF can be expressed in terms of $\mathbf{q}_n^{m/2}$ as:

$$[\overline{\mathbf{D}}_{n+1/2} \quad \tilde{\mathbf{D}}_{n+1/2}]^T = \left[(\mathbf{N_s}^{t_{n+1/2}})^T \mathbf{M_A} \mathbf{N_s}^{t_{n+1/2}}\right]^{-1} (\mathbf{N_s}^{t_{n+1/2}})^T \mathbf{M_A} \mathbf{q}_n^{m/2} \quad (57)$$

4.3 Coupling Scheme

Based on the two-way information passing between the MD and extended space-time FEM simulation, the two approaches are tied together in following way:

1. The MD simulation receives the information regarding the location of the ghost atoms from the extended space-time FEM simulation.
2. The extended space-time FEM simulation gets its initial conditions from the projection of the atomic displacements. The nodal DOFs of the extended space-time FEM simulation that correspond to the MD region are corrected at each coarse scale time step by using the projection operator on the MD solution at the appropriate MD sub-step.

The algorithm for the coupled extended space-time FEM-MD simulation using projection is as follows:

1. Apply initial displacements to the atoms in the MD region. Obtain the projection of these displacements onto the enriched nodal DOF and apply it as the initial condition for the extended space-time FEM simulation.
2. Assemble the extended space-time FEM stiffness matrices and advance the extended space-time FEM simulation through one time step.
3. Advance the MD simulation through m sub-steps. For each sub-step obtain the boundary information for the ghost atoms by interpolating the extended space-time FEM simulation nodal DOFs.
4. At the end of sub-step $m/2$ and m obtain a projection of the MD solution and replace the corresponding nodal DOFs from the extended space-time FEM simulation based on the projection.
5. Return to step 2 and continue till end of the simulation is reached.

5 Numerical Examples

In implementing the developed approach outlined in the last sections, we will focus on two cases. In the first case the interaction between the atoms is governed by a linear harmonic potential with spring constant k. In the second case the form of Lennard-Jones (LJ) potential is employed. The functional form of the LJ potential is given by:

$$\mathbf{U} = 4\varepsilon \left[\left(\frac{\sigma}{r}\right)^{12} - \left(\frac{\sigma}{r}\right)^{6}\right] \quad (58)$$

where r is the distance between the interacting atoms. ε and σ are LJ potential parameters. In this case, the stiffness value used for the coarse scale simulation is:

$$k = \frac{\partial^2 \mathbf{U}}{\partial r^2} = 24\varepsilon \left[26\frac{\sigma^{12}}{r^{14}} - 7\frac{\sigma^6}{r^8}\right] \quad (59)$$

k is evaluated at $r = r_e$, where r_e is the equilibrium spacing between the atoms which is $r_e = 2^{1/6}\sigma$. Finally, we note that the interaction is limited to the nearest neighbors only in both cases.

5.1 Linear Harmonic Potential

The configuration of the problem here is exactly the same as the one described in section 2. The discretization scheme is already shown in Figure

6 and the same combination of coarse plus fine scale wave profile as described by Eq.(29) is imposed (see Figure 7). The choice of the enrichment function is based on the fact that the total displacement is due to a combination of two waves, one traveling in the positive x direction and one in the negative x direction. These two waves initially overlap in a region from $-L_c$ to L_c. As the simulation progresses the region of overlap decreases. we propose to use two enrichment functions, $\phi_2(x,t)$ for the overlap case and $\phi_1(x,t)$ for the separated wave, where:

$$\phi_1(x,t) = \cos(b(|\,x\,| - ct)) \quad (|\,x\,| + ct > L_c) \tag{60}$$

$$\phi_2(x,t) = \cos(bx)\cos(bct) \quad (|\,x\,| + ct \leq L_c) \tag{61}$$

in which c is the speed of wave propagation and is governed by the dispersion relation. It is related to the wave number through

$$c = V_\infty \frac{|\sin(bh_a/2)|}{(bh_a/2)} \tag{62}$$

with $b = \frac{B\pi}{2Lc}$ and V_∞ is the velocity for a wave having infinite wavelength. As we have noted earlier, the interference region due to overlap reduces in size with the passage of time. In order to properly enrich the domain we would need to track this interference region. All the elements that are either completely or partially within the interference region would need to be enriched using ϕ_2. We first examine the ability of the developed method in eliminating the spurious wave reflections. The displacements for the two MD regions and the nodal displacements are plotted in Figure 15 for the same instant as in Figure 8. One can conclude from Figure 15 that the combination of the the BSM treatment and the multiscale enrichment approximation leads to a reflectionless interface. In Figure 15, we also observe that the atoms in the second MD region receive the fine scale portion of the total displacement due to the use of the enrichment approximation in the space-time FEM region. Figure 16 further compares the atomic displacement history at $x = 0.9$ with full-scale MD and BSM with just the regular space-time FEM coupling with MD.

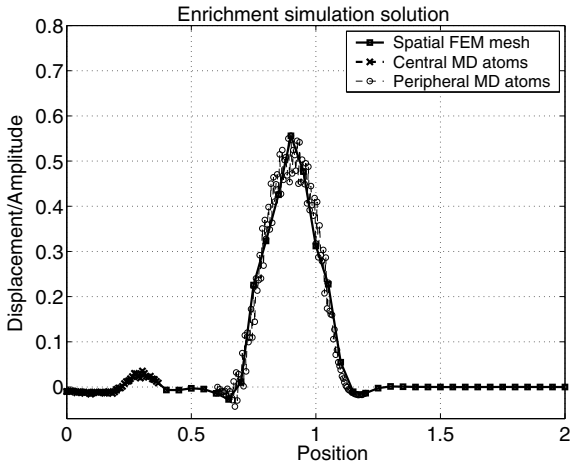

Figure 15: Enrichment solution displacement

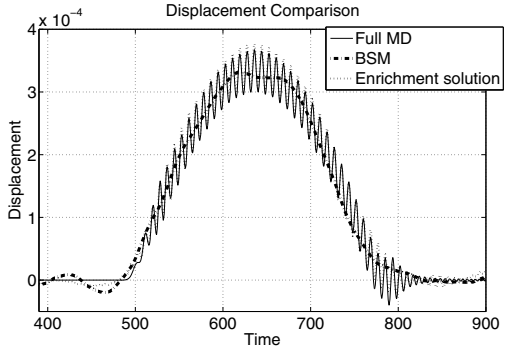

Figure 16: Comparison of displacement history for an atom at $x = 0.9$

As can be seen, without the enrichment, only the average response is captured with just the application of BSM. Thus, the importance of introducing the fine scale wave into the space-time FEM approximation is clearly demonstrated. Finally, we present a quantitative evaluation of the method in terms of the wave transmitting boundary condition. The energy history of the 2nd MD region resolved from the developed method is shown in Figure 17. Compared with the method using BSM in the case of coupling regular space-time FEM with MD, we observe dramatically different results. Without the enrichment, the amount of the energy flux in the 2nd MD region is less than 1% at its peak value. In contrast, the trajectory based on the enrichment solution fits well with the corresponding using full-scale MD, which is regarded

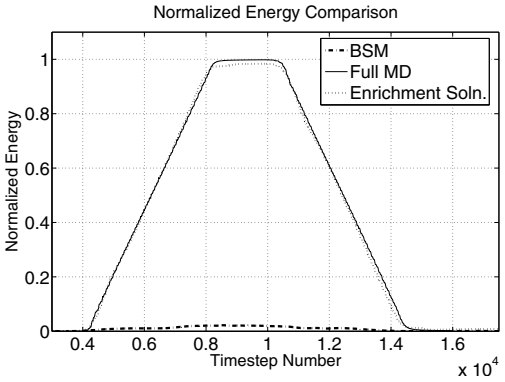

Figure 17: Comparison of normalized energy for the 2^{nd} MD region

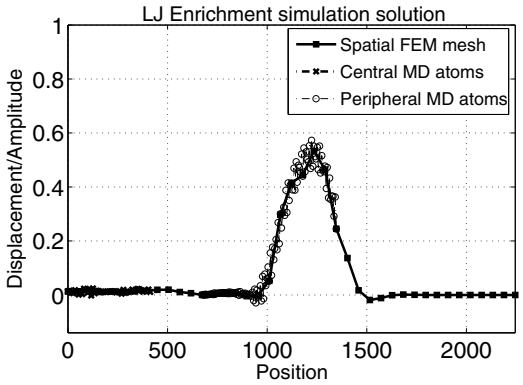

Figure 18: Enrichment solution displacement for LJ simulation

as the analytical solution in this case.

5.2 LJ Potential

The purpose of this case is to show that when the magnitude of the displacement is small compared with the lattice spacing, the proposed scheme also works well for nonlinear interactions. One possible application is analysis of lattice vibrations due to finite temperature effect, which consists of collection of phonons that are small in magnitude. In the current model, the LJ parameters are selected as $\varepsilon = 5$ and $\sigma = 1$. The equilibrium spacing thus becomes $r_e = 2^{1/6} = 1.1225$. The mass of each atoms is taken as $m_a = 10$. The total domain extends from -2244.924 to 2244.924 spanning 4001 atoms. The spatial domain is discretized using 161 nodes. The initial displacement is applied to a region extending from -224.4924 to 224.4924 (i.e. $L_c = 224.4924$).The initial displacement has the same form as Eq.(29). The main difference is that the amplitude of the disturbance, A is limited to $h_a/1000$.

Similar to the linear harmonic case the central MD region has 751 atoms and extends from -420.9232 to 420.9232. The peripheral MD region extends from 673.477 to 1346.9544 and spans 601 atoms. Figure 18 shows the displacement at 10800 MD steps. At this time, the wave already enters the second MD region. From Figure 18, it can be seen that the fine scale portion of the displacement passes out of the central MD region and is transmitted to the peripheral MD region. In Figure 19, the displacement of an atom in

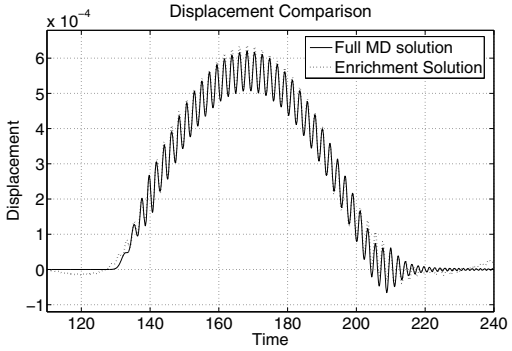

Figure 19: Predicted displacement for an atom at $x = 1010.215$

the peripheral MD region at $x = 1010.215$ as predicted by the proposed method is compared with that from the full MD simulation. The observation is similar to that in the linear case. The enrichment solution accurately predicts both the fine and coarse scale part of the response. Normalized energies for the two MD regions as predicted by the two different methods are also compared and shown in Figure 20. Here we observe some minor reflection that takes place at the interface. This can be attributed to linearity approximation made while solving the coarse scale simulation. Although further improvement can be made by implementing BSM approach, no additional treatment is carried out due to the fact that the amount of reflection is sufficiently small. In terms of the

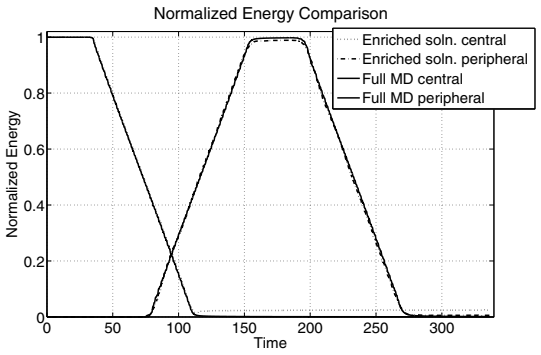

Figure 20: Normalized energy comparison for the 2 MD regions

wave transmitting condition, it can be seen that most of the energy are conveyed to the second MD region and it is very close to the full-scale MD case.

6 Summary

In summary, we have presented a new approach of treating the interface in coupled atomistic/continuum simulation. The proposed method is based on integrating the space-time finite element method with the enrichment approach. The unique features of coupling the multiscale space-time FEM with the atomistic simulation method are as follows: First of all, it provides a framework for representing the multiple scale phenomenon in both the spatial and temporal domains. Secondly, it enables one to directly address the time scales in coupled simulations as compared with the semi-discrete schemes. Lastly, the enrichment methodology allows for a more efficient representation of the particular physics when sufficient knowledge on the structure of the solutions is available. Such knowledge can be constructed from either analytical approaches or experimental observations. For instance, one could establish enrichment solution base on Green's function approach (e.g. Tewary and Read (2004); Yang and Tewary (2006, 2007)) in the case of modeling the nanostructures. It can also be combined with other multiscale techniques, e.g., (Ling and Alturi (2006); Ma, Liu, Lu, and Komaduri (2006); Shen and Alturi (2005, 2004a,b)) for resolving multiscale physics. In the current application, we have focused on wave propagations in small systems. The non-dissipative nature of the proposed method is clearly demonstrated in the example problems involving both linear systems and nonlinear systems. Finally, we would like to emphasize the fact that the framework presented is fairly general and not limited to wave propagation problems only. Many extensions can be made based on the developments presented in this paper. In particular, we believe the method is unique in treating engineering problems that are governed by mechanics and physics at multiple spatial and temporal scales.

7 Acknowledgment

The work presented is supported by the National Science Foundation grant No.0700107 and No.0600583 (Program Manager Dr. Clark Cooper). Any opinions, findings, conclusions, or recommendations expressed in this paper are those of the authors and do not necessarily reflect the views of the National Science Foundation. DQ would also like to thank Professor Ted Belytschko at Northwestern University for a critical review of the manuscript and providing a preprint of reference (Xu and Belytschko (2008)).

References

Argyris, J. H.; Scharpf, D. W. (1969): Finite elements in time and space. *The Aeronautical Journal of the Royal Aeronautical Society*, vol. 10, pp. 247–259.

Belytschko, T. (2007): *2nd DOE AtC workshop*.

Cai, W.; de Koning, M.; Bulatov, V. V.; Yip, S. (2000): Minimizing boundary reflections in coupled-Domain simulations. *Phys. Rev. Lett.*, vol. 85(15), pp. 3213–3216.

Chessa, J.; Belytschko, T. (2004): Arbitrary discontinuities in space-time finite elements by level sets and X-FEM. *International Journal for Numerical Methods In Engineering*, vol. 61), pp. 2595–2614.

Dolbow, J.; Moes, N.; Belytschko, T. (2000a): Discontinuous enrichment in finite elements with a partition of unity method. *Finite Elements in Analysis and Design*, vol. 36(3-4), pp. 235–260.

Dolbow, J.; Moes, N.; Belytschko, T. (2000b): Modeling fracture in Mindlin/Reissner plates with the extended finite element method. *International Journal of Solids and Structures*, vol. 37(48-50), pp. 7161–7183.

Duarte, C. A.; Babuška, I.; Oden, J. T. (2000): Generalized finite element methods for three-dimensional structural mechanics problems. *Computers & Structures*, vol. 77(2), pp. 215–232.

E, W.; Huang, Z. (2001): Matching conditions in atomistic-continuum modeling of materials. *Physical Review Letters*, vol. 87(13), pp. 135501.

E, W.; Huang, Z. (2002): A dynamic atomistic continuum method for the simulation of crystalline materials. *Journal of Computational Physics*, vol. 182(1), pp. 234–261.

Fried, I. (1969): Finite element analysis of time-dependent phenomena. *American Institute of Aeronautics and Astronautics*, vol. 7, pp. 1170–1173.

Gurtin, M. E. (1964): Variational principles for linear initial-value problems. *Quarterly of Applied Mathematics*, vol. 22, pp. 252–256.

Hughes, T. J. R.; Stewart, J. R. (1996): A space-time formulation for multiscale phenomena. *Journal of Computational and Applied Mathematics*, vol. 74(1-2), pp. 217–229.

Hulbert, G. M.; Hughes, T. J. R. (1990): Space-time finite element methods for second-order hyperbolic equations. *Computer Methods in Applied Mechanics and Engineering*, vol. 84(3), pp. 327–348.

Karpov, E. G.; Yu, H.; Park, H. S.; Liu, W. K.; Wang, Q. J.; Qian, D. (2006): Multiscale boundary conditions in crystalline solids: Theory and application to nanoindentation. *International Journal of Solids And Structures*, vol. 43(21), pp. 6359–6379.

Li, S.; Liu, X. H.; Agrawal, A.; To, A. C. (2005): Perfectly matched multiscale simulations for discrete systems: extension to multiple dimensions. *Physical Review B*, vol. 74, pp. 045418.

Li, X. D.; Wiberg, N. E. (1996): Structural dynamic analysis by a time-discontinuous galerkin finite element method. *International Journal for Numerical Methods in Engineering*, vol. 39(12), pp. 2131–2152.

Ling, X.; Alturi, S. N. (2006): A lattice-based cell model for calculating thermal capacity and expansion of single wall carbon nanotubes. *CMES: Computer Modeling in Engineering & Sciences*, vol. 14(2), pp. 91–100.

Liu, X. H.; Li, S. F. (2007): A non-equillibrium multiscale computational model. *Journal of Chemical Physics*, vol. 126, pp. 124105.

Ma, J.; Liu, Y.; Lu, H.; Komaduri, R. (2006): Multiscale simulation of nanoindentation using the generalized interpolation material point (GIMP) method, dislocation dynamics (DD) and molecular dynamics (MD). *CMES: Computer Modeling in Engineering & Sciences*, vol. 16(1), pp. 41–56.

Melenk, J. M.; Babuška, I. (1996): The partition of unity finite element method: Basic theory and applications. *Computer Methods in Applied Mechanics and Engineering*, vol. 139(1-4), pp. 289–314.

Oden, J. T. (1969): A general theory of finite elements II. Applications. *International Journal for Numerical Methods In Engineering*, vol. 1, pp. 247–259.

Park, H. S.; Karpov, E. G.; Liu, W. K.; Klein, P. A. (2005): The bridging scale for two-dimensional atomistic/continuum coupling. *Philosophical Magazine*, vol. 85(1), pp. 79–113.

Qian, D.; Gondhalekar, R. H. (2004): A virtual atom cluster approach to the mechanics of nanostructures. *International Journal for Multiscale Computational Engineering*, vol. 2(2)), pp. 277–289.

Qian, D.; Wagner, G. J.; Liu, W. K. (2004): A multiscale projection method for the analysis of carbon nanotubes. *Computer Methods in Applied Mechanics and Engineering*, vol. 193(17-20), pp. 1603–1632.

Shen, S. P.; Alturi, S. N. (2004a): Computational nano-mechanics and multi-scale simulation. *CMC: Computers, Materials & Continua*, vol. 1(1), pp. 59–90.

Shen, S. P.; Alturi, S. N. (2004b): Multiscale simulation based on the meshless local Petrov-Galerkin (MLPG) method. *CMES: Computer Modeling in Engineering & Sciences*, vol. 5(3), pp. 235–255.

Shen, S. P.; Alturi, S. N. (2005): A tangent stiffness MLPG method for atom/continuum multiscale simulation. *CMES: Computer Modeling in Engineering & Sciences*, vol. 7(1), pp. 49–67.

Sukumar, N.; Moes, N.; Moran, B.; Belytschko, T. (2000): Extended finite element method for three-dimensional crack modelling. *International Journal for Numerical Methods in Engineering*, vol. 48(11), pp. 1549–1570.

Tewary, V. K.; Read, D. T. (2004): Integrated green's function molecular dynamics method for multiscale modeling of nanostructures: application to Au nanoisland in Cu. *CMES: Computer Modeling in Engineering & Sciences*, vol. 6(4)), pp. 359–372.

To, A. C.; Li, S. (2005): Perfectly matched multiscale simulations. *Physical Review B*, vol. 72, pp. 035414.

Wagner, G. J.; Karpov, E. G.; Liu, W. K. (2004): Molecular dynamics boundary conditions for regular crystal lattices. *Computer Methods in Applied Mechanics and Engineering*, vol. 193(17-20), pp. 1579–1601.

Wagner, G. J.; Liu, W. K. (2003): Coupling of atomistic and continuum simulations using a bridging scale decomposition. *Journal of Computational Physics*, vol. 190, pp. 249–274.

Xiao, S. P.; Belytschko, T. (2004): A bridging domain method for coupling continua with molecular dynamics. *Computer Methods in Applied Mechanics and Engineering*, vol. 193(17-20), pp. 1645–1669.

Xu, M.; Belytschko, T. (2008): Conservation properties of the bridging domain method for coupled molecular/continuum dynamics. *International Journal for Numerical Methods In Engineering*, vol. in press.

Yang, B.; Tewary, V. K. (2006): Efficient green's function modeling of line and surface defects in multilayered anisotropic elastic and piezoelectric materials. *CMES: Computer Modeling in Engineering & Sciences*, vol. 15(3)), pp. 165–178.

Yang, B.; Tewary, V. K. (2007): Multiscale modeling of point defects in Si-Ge(001) quantum wells. *Physical Review B*, vol. 75(14)), pp. 144103.

Zienkiewicz, O. C.; Taylor, R. L.; Sherwin, S. J.; Peiro, J. (2003): On discontinuous Galerkin methods. *International Journal for Numerical Methods In Engineering*, vol. 58(8), pp. 1119–1148.